European Journal of Computational Mechanics, 2014
Vol. 23, Nos. 1–2, 61–77, http://dx.doi.org/10.1080/17797179.2014.912072

Taylor & Francis
Taylor & Francis Group

Buoyancy-driven heat transfer analysis in a square cavity with a mounted variable length partition in the presence of magnetic field

Arab Solghar[a]* and M. Davoudian[b,c]

[a]*Faculty of Engineering, Department of Mechanical Engineering, Vali-e-Asr University, Rafsanjan, Iran;* [b]*Mechanical Branch, Department of Engineering, Islamic Azad University, Izeh, Iran;* [c]*Faculty of Engineering, Department of Mechanical Engineering, Shahrekord University, Shahrekord, Iran*

In this study, steady, laminar, natural-convection flow in the presence of a magnetic field in a square enclosure with vertical partition, heated from left and cooled from right is considered. The horizontal walls are well insulated. The cavity is filled with Al_2O_3–water nanofluid. To consider the influence of magnetic force, a horizontal magnetic field is externally imposed on the left wall. The basic nonlinear differential equations describing the flow driven by natural convection consist of continuity, momentum and energy which are solved numerically utilising finite volume code based on PATANKAR's SIMPLER method. It is found that for a given condition, the height of vertical partition has strong effect upon flow field and the rate of heat transfer. Also it is shown that Nusselt number of hot wall varies remarkably with volume fraction of nanoparticles in base fluid and changes differently at low, medium and high Rayleigh number.

Keywords: free convection; nanofluid; cavity; baffle; MHD

1. Introduction

The study of natural convection in cavities has been the topics of many researches in the recent years because of its significant applications in nature and in engineering implication. Enclosures with vertical partitions have important application in various scientific and engineering practices particularly in the cooling systems of electronic components, the building and thermal insulation systems, the built-in storage solar collectors, the nuclear reactor systems, the food storage industry and the geophysical fluid mechanics. A few numerical and experimental studies have been devoted on this subject.

Ampofo (2004) experimentally investigated low-level turbulent natural convection in an air-filled vertical-partitioned square enclosure. The local velocity and temperature were measured at different locations in the cavity. Oztop, Dagtekin, and Bahloul (2004) studied the effect of heated thin plate location in a cavity on natural heat convection and found that heat transfer is enhanced with the vertical plate.

Bilgen (2005) dealt with numerical analysis of a differentially heated square cavity filled with thin conductive fin on the hot wall. He observed that Nusselt number decreased by reducing fin length and relative conductivity ratio. Also, the heat transfer by natural convection was minimised when fin was at the centre or near the centre of cavity. Ambarita et al. (2006) numerically investigated the flow field and heat transfer

*Corresponding author. Email: a.arabsolghar@vru.ac.ir

for differentially heated square enclosure. Two insulated baffles attached to adiabatic horizontal walls were considered in that study. The resultant Nusselt number varies with both baffles positions and inclination angles of cavity.

An experimental study of the natural convection heat transfer and fluid flow in horizontal and vertical narrow enclosures with heated rectangular finned plate at a wide range of Rayleigh numbers for different values of spacing and fin length was carried out by Nada (2007). He found that the insertion of heat-conducting fins always enhances heat transfer rate. The results presented an optimum fin spacing at which Nusselt number and finned surface effectiveness were maximum.

Ben-Nakhi and Chamkha (2007) investigated natural convection in a square enclosure with an inclined conductive thin fin attached to the middle of the left thin wall. The left wall was hot and the external sides of three other thick walls were cold. It was found that, in general, the thin fin reduces the mean Nusselt number.

Kahveci and Oztuna (2008) examined the effect of magnetic field on the flow and heat transfer in an inclined cavity with a centred partition and found that for high Rayleigh numbers, the average Nusselt number shows an increasing trend as the tilting angle increases and a peak value is detected. They found that the Prandtl number has only a marginal effect on the flow and heat transfer. Kandaswamy, Lee, Abdul Hakeem, and Saravanan (2008) examined buoyancy-driven convection in a square cavity with two mutually orthogonal located thin baffles. They concluded that heat transfer in the cavity augmented by increasing baffle length and cavity ratio. In addition, upward movement of horizontal baffle led to decrease in heat transfer.

Saravanan, Abdul Hakeem, Kandaswamy, and Lee (2008) dealt with buoyancy-driven convection in a square cavity induced by two mutually orthogonal heated thin plates under isothermal and isoflux boundary conditions. They demonstrated that the resulting convection pattern is stronger for the isothermal boundary condition. It was also deduced that a better overall heat transfer can be achieved by placing one of the plates far away from the centre of the cavity for isothermal boundary condition and near the centre of the cavity for isoflux boundary condition.

Saravanan, Abdul Hakeem, and Kandaswamy (2009) numerically studied natural convection in a cavity induced by two mutually orthogonal heat-generating baffles. They found that when both baffles were mounted inside the cavity, an increase in the length of any of the baffle results in a proportionate increase in the overall heat transfer rate. But no significant changes in the overall heat transfer rate occur for different positions of the baffles.

Anderson, Duke, and Carson (2010) conducted an experimental study and showed that the use of a single baffle is as a possible low-cost means of suppressing heat loss by natural convection in an attic-shaped enclosure. It was found that the heat transfer coefficient changes with baffle length.

Mahmoodi (2011) dealt with the free convection fluid flow and heat transfer of various water-based nanofluids in a square cavity with an inside thin heater. It was deduced that at low Rayleigh numbers the horizontal positioned heater has higher Nusselt number compared to the vertically positioned heater, while at high Rayleigh numbers the position of the heater does not affect the heat transfer rate. Also, for a horizontal heater when it is located in lower half of the cavity, more heat transfer occurs compared to the case of heater located in upper half of the cavity. Moreover, it was found that at high Rayleigh numbers, the Ag–water nanofluid is more effective to enhance the heat transfer rate while at low Rayleigh numbers the type of nanofluids does not affect the heat transfer rate.

Wang, Shi, and Li (2012) studied numerically the natural convection heat transfer from a heated thin plate located in the middle of a lid-driven inclined square enclosure. The study is formulated in terms of the vorticity-stream function procedure and numerical solution was performed using a fully higher order compact finite difference scheme. They found that fluid flow and temperature fields strongly depend on Rayleigh numbers and inclination angles.

Arefmanesh, Najafi, and Musavi (2013) utilised the meshless local Petrov–Galerkin method for the simulation of the buoyancy-driven flow and heat transfer in a differentially heated enclosure with a baffle attached to its higher temperature side wall. Their study indicated the vital role of the baffle in transferring heat from the hot wall. They found that elevating the location of the baffle on the hot wall increases the average hot wall Nusselt number. It was found that the heat transfer across the cavities can be adjusted by changing the physical and geometrical constraints.

From the above literature reviews, it can be seen that there are plenty of studies using numerical methods on free convection in rectangular cavities with different boundary conditions and with partition(s) mounted inside enclosure. To the best of authors' knowledge, no study has been dealt with the investigation of buoyancy-driven fluid flow and heat transfer in a square cavity with a centrally vertical-variable length partition under the influence of magnetic field. In the present work, the container is filled with Al_2O_3–water nanofluid. The coupled governing equations are dicretised through finite volume method and solved using SIMPLER algorithm. The results are illustrated in the form of streamlines and isotherms plots, average Nusselt number and local Nusselt number for a wide range of Rayleigh number, volume fraction of the nanoparticles and different length of partition.

2. Problem formulation

Consider the steady laminar two-dimensional flow of a nanofluid in a square cavity of height H in the presence of an applied horizontal magnetic field (Figure 1). The two horizontal walls are well insulated. The left and right vertical walls are maintained at hot (T_h) and cold (T_c) temperatures, respectively. The fluid is a water-based nanofluid containing alumina (Al_2O_3) nanoparticles. The thermophysical properties of the pure fluid and the solid particles are listed in Table 1. The nanofluid used in this study is

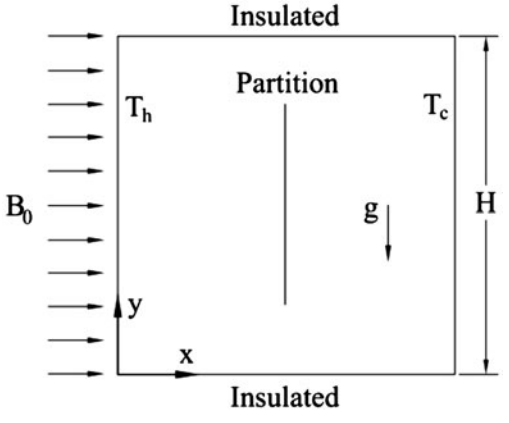

Figure 1. Physical configuration.

assumed to be Newtonian and incompressible and the flow is laminar. Moreover, it is assumed that the base fluid and the nanoparticles are in thermal equilibrium and they flow at same velocity. The induced magnetic field is assumed to be negligible compared to the applied magnetic field. The length of the cavity perpendicular to the plane of the geometry is assumed to be long enough; therefore, the problem is considered two-dimensionally.

The continuity, momentum and energy equations for two-dimensional problem of steady state laminar free convection in a cavity are:

$$\frac{\partial u}{\partial x}+\frac{\partial v}{\partial y}=0 \tag{1}$$

$$u\frac{\partial u}{\partial x}+v\frac{\partial u}{\partial y}=-\frac{1}{\rho_{nf}}\frac{\partial p}{\partial x}+\frac{\mu_{nf}}{\rho_{nf}}\left(\frac{\partial^2 u}{\partial x^2}+\frac{\partial^2 u}{\partial y^2}\right) \tag{2}$$

$$u\frac{\partial v}{\partial x}+v\frac{\partial v}{\partial y}=-\frac{1}{\rho_{nf}}\frac{\partial p}{\partial y}+\frac{\mu_{nf}}{\rho_{nf}}\left(\frac{\partial^2 v}{\partial x^2}+\frac{\partial^2 v}{\partial y^2}\right)+\frac{(\rho\beta)_{nf}}{\rho_{nf}}g\,(T-T_c)-\frac{\sigma_{nf}B^2}{\rho_{nf}}v \tag{3}$$

and

$$u\frac{\partial T}{\partial x}+v\frac{\partial T}{\partial y}=\frac{k_{nf}}{(\rho C_p)_{nf}}\left(\frac{\partial^2 T}{\partial x^2}+\frac{\partial^2 T}{\partial y^2}\right) \tag{4}$$

where the effective density, electrical conductivity, thermal expansion coefficient and heat capacity of the nanofluid are obtained as following:

$$\rho_{nf}=(1-\varphi)\,\rho_f+\varphi\rho_p \tag{5}$$

$$\sigma_{nf}=(1-\varphi)\,\sigma_f+\varphi\sigma_p \tag{6}$$

$$(\rho\beta)_{nf}=(1-\varphi)\,(\rho\beta)_f+\varphi\,(\rho\beta)_p \tag{7}$$

$$(\rho C_p)_{nf}=(1-\varphi)\,(\rho C_p)_f+\varphi\,(\rho C_p)_p \tag{8}$$

with φ being the volume fraction of the solid nanoparticles and subscripts f, nf and P stand for base fluid, nanofluid and particle, respectively.

The Brinkman model (Brinkman, 1952) is employed for the computation of nanofluid viscosity. According to this model for the two-phase mixture, the viscosity of the nanofluid is obtained from the following relation:

$$\mu_{nf}=\frac{\mu_f}{(1-\varphi)^{2.5}} \tag{9}$$

Table 1. Thermophysical properties of different phases (Oztop & Abu-Nada, 2008).

Physical properties	Fluid phase (water)	Solid phase (Al_2O_3)
C_P (J/kg K)	4179	765
ρ (kg/m^3)	997.1	3970
k (W/m K)	0.613	40
α (m^2/s)	1.471×10^{-7}	1.32×10^{-5}
β (K^{-1})	2.761×10^{-5}	0.85×10^{-5}

The effective thermal conductivity of the nanofluid is determined using the Maxwell–Garnett's model (Maxwell-Garnett, 1904). For a suspended spherical nanoparticle in a base fluid, the conductivity is given as

$$k_{nf} = k_f \left[\frac{(k_p + 2k_f) - 2\,\varphi(k_f - k_p)}{(k_p + 2k_f) + \varphi(k_f - k_p)} \right] \tag{10}$$

Using the following non-dimensional variables:

$$X = \frac{x}{H},\quad Y = \frac{Y}{H},\quad U = \frac{uH}{\alpha_f},\quad V = \frac{vH}{\alpha_f},\quad P = \frac{pL^2}{\rho_{nf}\alpha_f^2},\quad \theta = \frac{T - T_c}{T_h - T_c} \tag{11}$$

The governing Equations (1)–(4) reduce to dimensionless form as

$$\frac{\partial U}{\partial X} + \frac{\partial V}{\partial Y} = 0 \tag{12}$$

$$U\frac{\partial U}{\partial X} + V\frac{\partial U}{\partial Y} = -\frac{\partial P}{\partial X} + \frac{\mu_{nf}}{\rho_{nf}\alpha_{nf}}\left(\frac{\partial^2 U}{\partial X^2} + \frac{\partial^2 U}{\partial Y^2}\right) \tag{13}$$

$$U\frac{\partial V}{\partial X} + V\frac{\partial U}{\partial Y} = -\frac{\partial P}{\partial Y} + \frac{\mu_{nf}}{\rho_{nf}\alpha_{nf}}\left(\frac{\partial^2 V}{\partial X^2} + \frac{\partial^2 V}{\partial Y^2}\right) + \frac{(\rho\beta)_{nf}}{\rho_{nf}\beta_f} Ra\,Pr\,\theta - Ha^2 Pr\,V \tag{14}$$

and

$$U\frac{\partial \theta}{\partial X} + V\frac{\partial \theta}{\partial Y} = \frac{\alpha_{nf}}{\alpha_f}\left(\frac{\partial^2 \theta}{\partial X^2} + \frac{\partial^2 \theta}{\partial Y^2}\right) \tag{15}$$

The expressions for dimensionless parameters are given as

$$Ha = B_0 H\sqrt{\frac{\sigma_{nf}}{\nu_f\,\rho_{nf}}},\quad Pr = \frac{\nu_f}{\alpha_f},\quad Ra = \frac{g\beta_f H^3(T_h - T_c)}{\nu_f\,\alpha_f} \tag{16}$$

Dimensionless boundary conditions used to solve the system of Equations (12)–(15) are as

$$\begin{array}{lll} X = 0 & \rightarrow & U = V = 0\,,\quad \theta = 1 \\ X = 1 & \rightarrow & U = V = 0\,,\quad \theta = 0 \\ Y = 0 & \rightarrow & U = V = 0\,,\quad \partial\theta/\partial Y = 0 \\ Y = 1 & \rightarrow & U = V = 0\,,\quad \partial\theta/\partial Y = 0 \end{array} \tag{17}$$

Also on the partition, no slip boundary condition is applied. It is assumed that its thickness is negligible, so no thermal boundary condition is required.

The local Nusselt number of the walls is calculated via

$$Nu = \frac{hH}{k_f} \tag{18}$$

where the heat transfer coefficient is given as

$$h = \frac{q_w}{(T_h - T_c)} \tag{19}$$

The thermal conductivity is written as

$$k_{nf} = -\frac{q_w}{\partial T/\partial x} \tag{20}$$

Substitution of Equations (19) and (20) into Equation (18) yields the following equation for the local Nusselt number:

$$Nu_Y = -\frac{k_{nf}}{k_f}\left(\frac{\partial\theta}{\partial X}\right)_{X=0} \tag{21}$$

The average Nusselt number of the left wall is obtained by the integration of the local Nusselt number along the walls as follows:

$$Nu_m = -\frac{1}{H}\int_0^1 Nu_Y dY \tag{22}$$

3. Grid testing and code validation

The governing continuity, momentum and energy equations were solved through control volume method using uniform meshes. The SIMPLER algorithm has been applied for the pressure velocity coupling. The diffusion terms in the equations are discretised by the second-order central difference scheme while the hybrid scheme (combination of the central difference scheme and the upwind scheme) is employed to approximate the convection terms. The set of discretised equations are solved by tri-diagonal matrix algorithm line-by-line method. A staggered grid system, in which the velocity components are stored midway between the scalar storage locations, is used. The convergence of solutions is obtained when the relative error for each variable between consecutive iterations is recorded below 10^{-6}.

In order to obtain grid independent solution, a grid refinement study is performed on a square cavity with $Hm = 0.5$, $Ra = 10^5$ and $Ha = 30$ containing Al_2O_3–water nanofluid with $\varphi = 0.03$. Therefore, six combinations (21×21, 41×41, 61×61, 81×81, 101×101 and 121×121) of control volumes are used to test the effect of grid size on the precision of the predicted results. The convergence of the average Nusselt number on the left wall and the maximum stream-function with grid refinement are depicted in Figure 2(a) and (b), respectively. It is observed that grid independence is achieved with combination of (101×101) control volumes where no further change is observed in those parameters with the improvement of finer grid.

In order to verify the accuracy of the present numerical study, the proposed numerical scheme was validated by performing simulations for the classical natural convection in an air-filled square cavity carried out by De Vhal Davies (1983), Markatos and pericleous (1984), Barakos, Mitoulis, and Assimacopoulos (1994) and Khanafer, Vafai, and Lightstone (2003) as shown in Table 2. Moreover, the present computational method is also verified by the study of Ghasemi, Aminossadati, and Raisi (2001) for natural convection in a square cavity under magnetic force containing nanofluid for $Ra = 10^3$ as illustrated in Figure 3. All of these comparisons insure the accuracy of the numerical results of the present work.

4. Results and discussions

In this section, the numerical results for natural convection heat transfer in an enclosure with zero thickness partition are discussed. The non-dimensional controlling parameters for this investigation are the Rayleigh number Ra, partition height Hm and volume fraction of nanoparticle φ. Throughout the study, the Hartman number is kept constant at

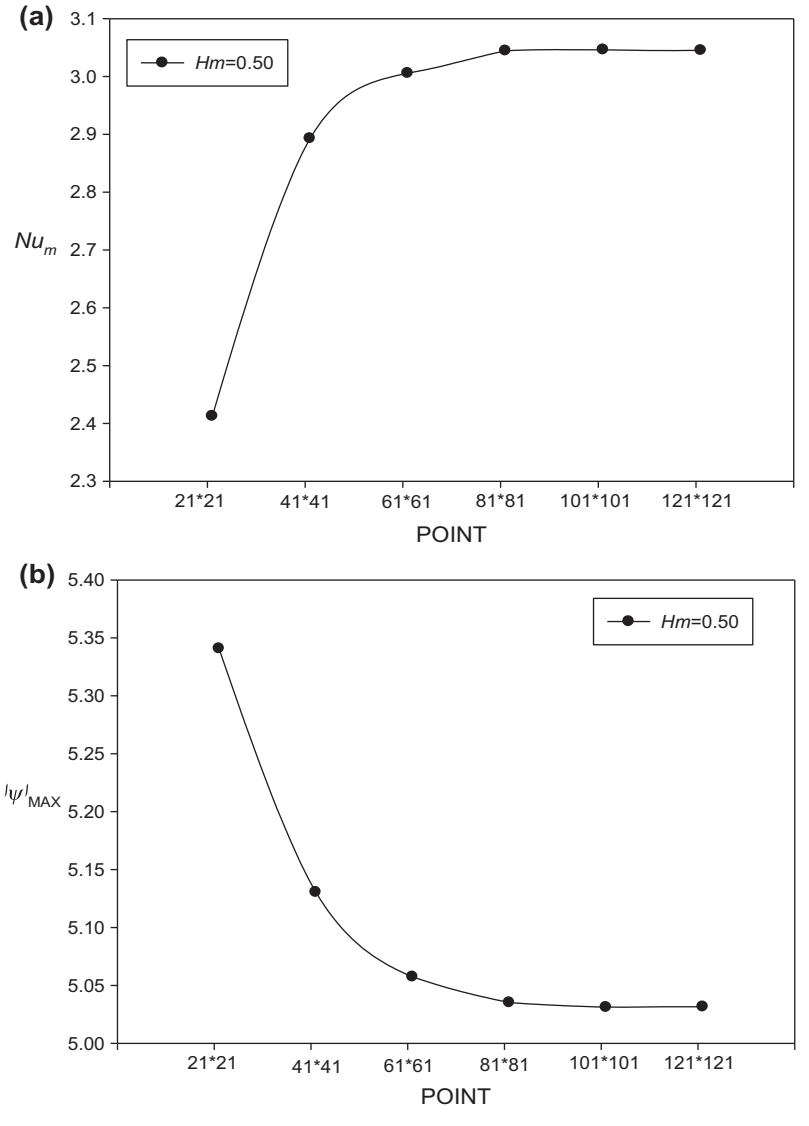

Figure 2. Grid test for (a) The average Nusselt number on the left wall; (b) The average stream function.

Table 2. The average Nusselt number on the hot wall for a square cavity filled with air.

	Ra			
	10^3	10^4	10^5	10^6
Present work	1.115	2.225	4.523	8.813
De Vahl Davise (1983)	1.118	2.243	4.519	8.719
Markatos and pericleous (1984)	1.108	2.201	4.430	8.754
Barakos, Mitoulis, and Assimacopoulos (1994)	1.114	2.245	4.510	8.806
Khanafer et al. (2003)	1.118	2.245	4.522	8.829

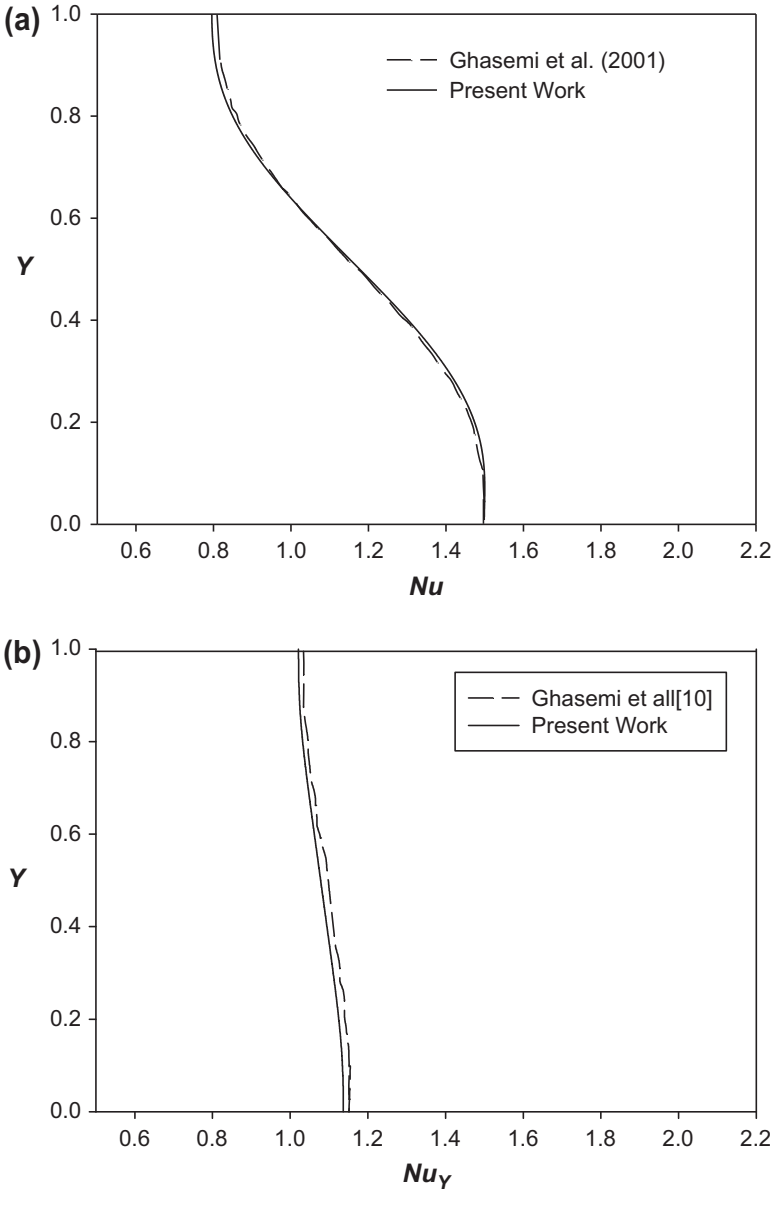

Figure 3. The Nusselt number of hot wall for (a) $Ha = 0$; (b) $Ha = 30$.

30. Besides, the value of Ra is varied from 10^3 to 10^6 to cover a wide range of Rayleigh number. Moreover, calculations were carried out for a few values of volume fraction of nanoparticles ($\varphi = 0.01$, 0.03, 0.05 and 0.07) and partition height ($Hm = 0$, 0.2, 0.4, 0.6, 0.8 and 0.96).

In order to study the effect of partition height on the flow field, isotherms and streamlines are plotted for different values of partition height ranging from 0 to 0.96, while the other pertinent parameters are maintained constant ($\varphi = 0.03$, $Ha = 30$ and $Ra = 10^5$). As seen in Figure 4, in the absence of vertical partition, there is only one

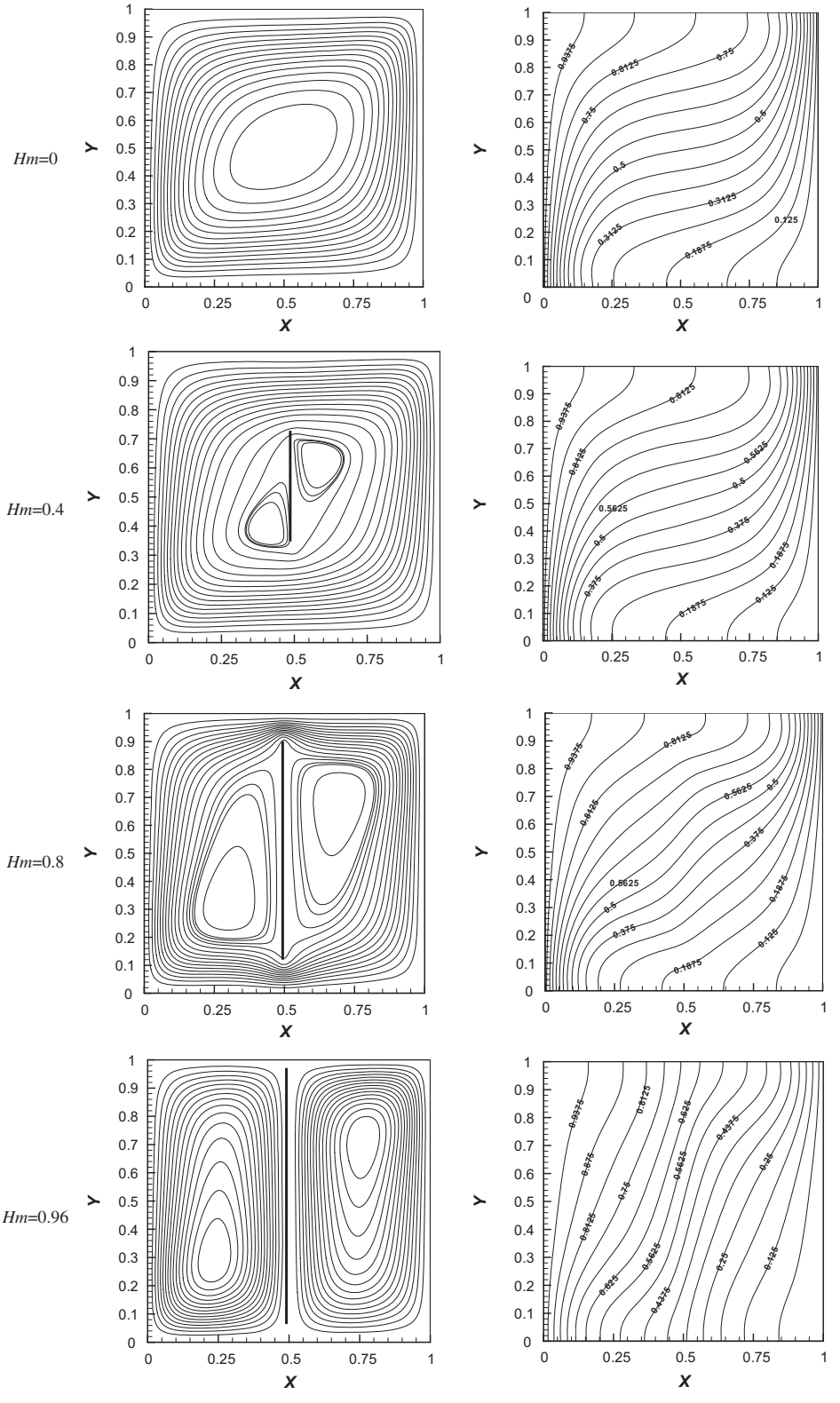

Figure 4. The streamlines (left) and isotherms (right) as functions of partition height.

vortex rotating CW. As a partition is centrally mounted inside the cavity, two vortexes are formed around the plate. Because on the plate, no slip boundary condition is applied, consequently vortexes are divided by the plate. In addition, there is a larger vortex in cavity which surrounds smaller vortexes near the partition.

As the height of partition increases, the stronger vortexes are formed close to it, such that for the case of $Hm = 0.96$, there are just two large vortexes and the partition prevents the fluid to flow through the gap between vertical plate and the horizontal walls of the cavity.

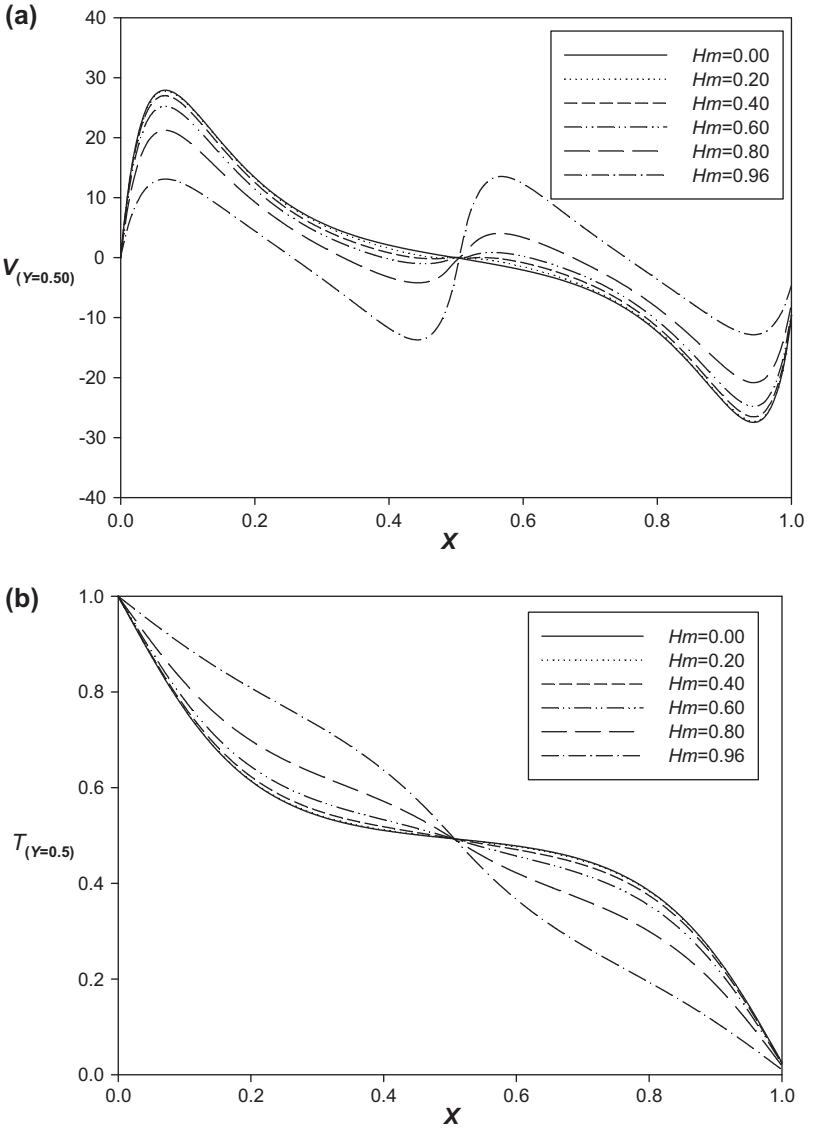

Figure 5. The influence of vertical partition height on (a) vertical velocity; (b) temperature profile.

From Figure 4 it can be observed that the slope of isotherms to the horizon increases with the partition height, because the increase of partition height slows down the flow, consequently heat transfer occurs mainly through conduction. Furthermore, temperature and vertical velocity profiles along x-axis at $Y = 0.5$ are depicted in Figure 5. The sinuous profiles of vertical velocity illustrate the direction of flow rotation. Close to the hot wall, the fluid ascends while close to the cold wall, the fluid descends. According to Figure 5, as the height of middle partition increases, the absolute value of vertical velocity reduces. Moreover, the inflexion point on each curve indicates the variation of direction of rotation. It is noted that the reduction of flow velocity attenuates the maximum stream function as shown in Table 3. Comparing the temperature profiles of Figure 5(b) it is disclosed that the curves become smoother and almost linear when the size of partition increases. This trend is consistent with the results of Figure 6 which state that the Nusselt number of hot wall reduces with the increase of partition height.

Figure 7 represents the variation of normalised Nusselt number with Rayleigh number. As seen, at low Ra ($10^3 \le Ra \le 10^5$) the increase of Rayleigh number leads to the reduction of Nusselt number. However, at $Ra = 10^6$, the Nusselt number augments, since at high Ra, convection heat transfer dominates mechanism.

The effect of volume fraction of nanoparticles on the absolute values of stream function ($|\psi|_{max}$) is presented in Table 4. The results are prepared for $Ha = 30$, $Hm = 0.7$, $0.01 \le \varphi \le 0.07$ and $10^3 \le Ra \le 10^6$. Apparently from Table 4, at $Ra \le 10^5$, the increase of nanoparticles volume fraction reduces the absolute values of stream function. Because it raises the flow viscosity, thus the circulation of nanofluid is

Table 3. The maximum stream functions at different heights of partition.

Hm	0.00	0.20	0.40	0.60	0.80	0.96
$\|\psi\|_{max}$	5.57	5.45	5.20	4.78	3.92	2.24

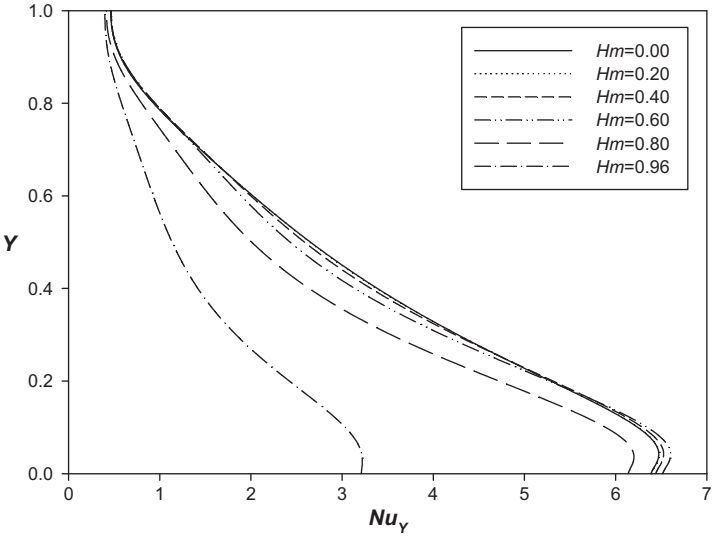

Figure 6. The variation of local Nusselt number of hot wall.

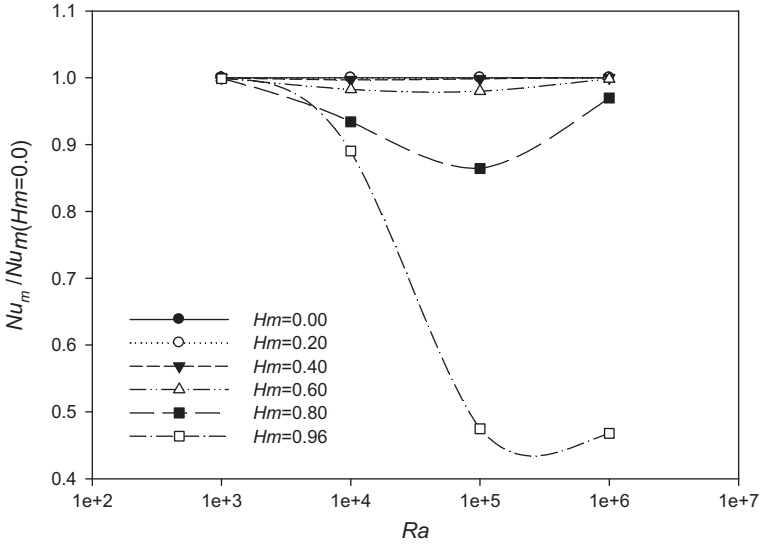

Figure 7. The normalised Nusselt number vs. Rayleigh number.

Table 4. The maximum stream functions at different nanoparticles volume fraction and Rayleigh numbers.

	φ			
Ra	0.01	0.03	0.05	0.07
10^3	0.083	0.077	0.072	0.067
10^4	0.812	0.762	0.714	0.670
10^5	4.567	4.501	4.425	4.435
10^6	12.639	12.801	12.971	13.119

lowered, leading to the decrease of $|\psi|_{max}$. Whereas the adverse trend is observed for $Ra = 10^6$. In Figure 8, the streamlines are simultaneously displayed for $\varphi = 0.01$ and $\varphi = 0.07$ in solid and dash line, respectively.

The variation of vertical velocity profiles and Nusselt number of hot wall for different values of nanoparticles volume fraction and Rayleigh number are illustrated in Figures 9 and 10, respectively. It is observed from Figure 9 that in all cases, the flow velocity reduces as the volume fraction of nanoparticles increases. Also, the flow velocity changes remarkably with the variation of Rayleigh number. At $Ra \leq 10^4$, buoyancy forces are weak and most of heat transfers via conduction. Obviously from Figure 10, the rate of heat transfer increases as the volume fraction of nanoparticle increases (as shown in Table 5). This is due to the increase of nanofluid conductivity. An interesting result is detected at $Ra = 10^5$, in which the rate of heat transfer reduces with the rise of volume fraction of nanoparticle. In one hand, with the increase of nanoparticle volume fraction, the flow is decelerated due to the increase of fluid viscosity which reduces the convection, on the other hand, the increase of nanoparticle volume fraction

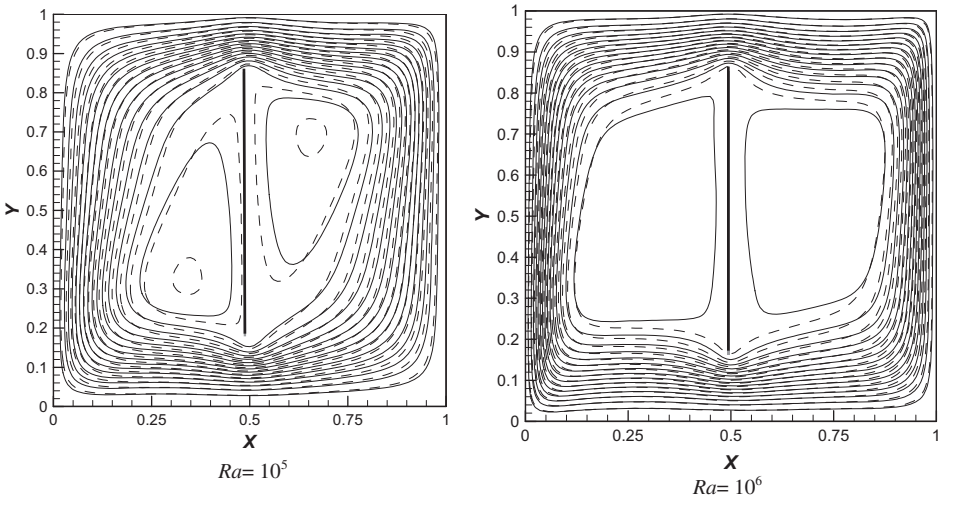

Figure 8. The comparison between streamlines for $\varphi = 0.01$ (——) and $\varphi = 0.07$ (– – – –).

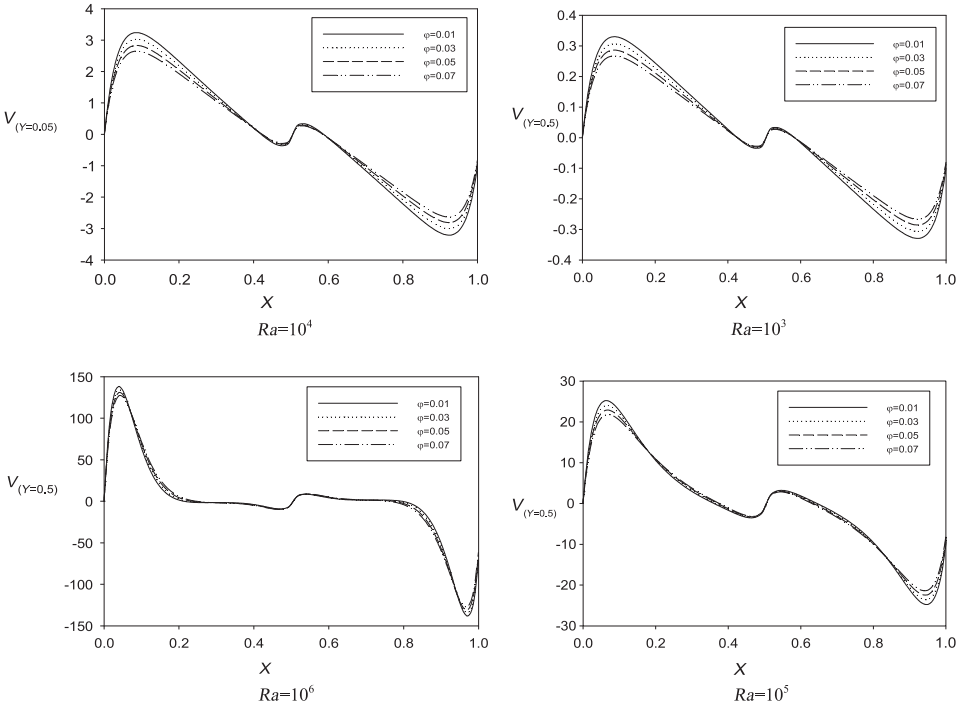

Figure 9. The vertical velocity along x-axis at $Y = 0.5$.

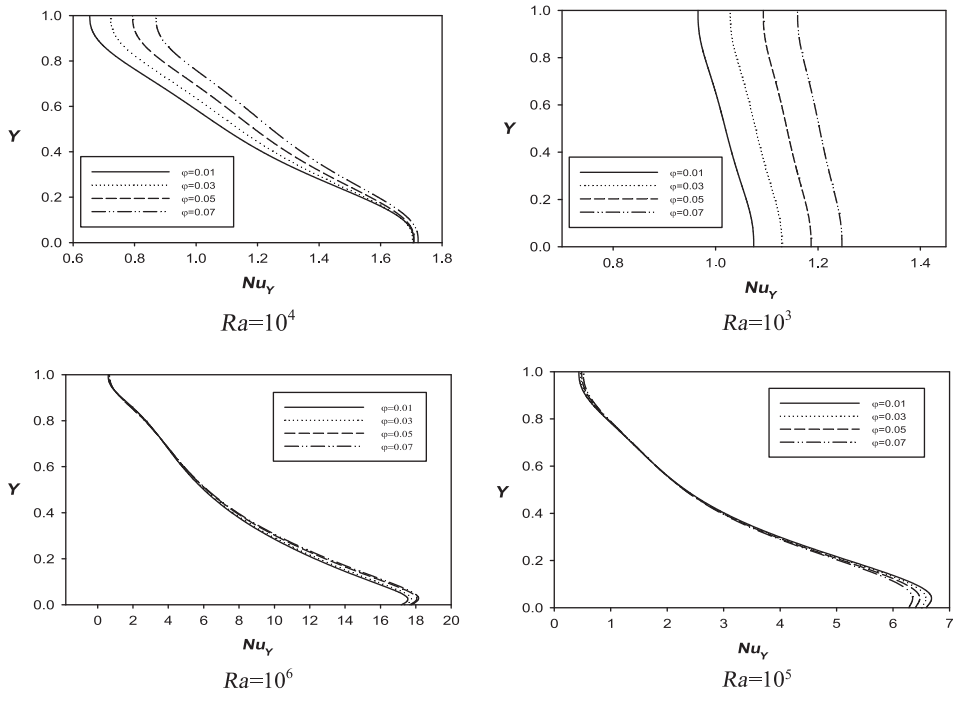

Figure 10. The local Nusselt number along x-axis at $Y = 0.5$.

Table 5. The average Nusselt number at different nanoparticles volume fraction and Rayleigh numbers.

	φ			
Ra	0.01	0.03	0.05	0.07
10^3	1.020	1.078	1.139	1.203
10^4	1.141	1.180	1.224	1.273
10^5	2.946	2.925	2.902	2.877
10^6	7.369	7.460	7.540	7.611

increases conductivity of fluid and augments conduction heat transfer, but the combination of these effects reduces overall heat transfer at $Ra = 10^5$ as seen in Table 5.

At $Ra = 10^6$, the rate of heat transfer rises with the increase of nanoparticle volume fraction. The same results were observed by Ghasemi et al. (2001), Aminossadati and Ghasemi (2009) and Ho, Chen, and Li et al. (2008).

Figure 11 demonstrates that at $Ra \leq 10^4$, the rate of heat transfer increases with the volume fraction of nanoparticle. The opposite happened for the case of $Ra = 10^5$. Moreover, the influence of the nanoparticle volume fraction is more pronounced at low Rayleigh number.

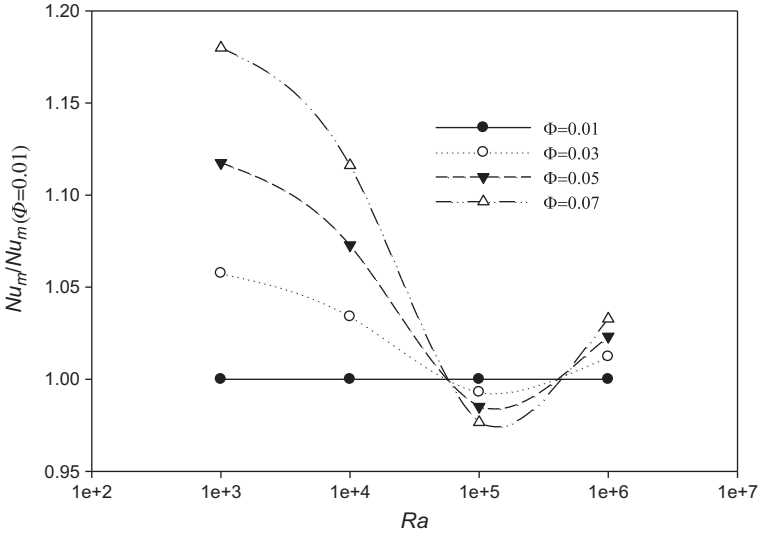

Figure 11. The normalised Nusselt number vs. Rayleigh number.

5. Conclusions

In this study, free convection heat transfer was examined in a cavity with vertical partition. The coupled governing equations were discretised through control volume method and simultaneously solved using SIMPLER algorithm. The analyses were carried out for different values of partition height, Rayleigh number and volume fraction of nanoparticle. Below conclusions can be drawn from present work:

With the lengthening of middle partition, the flow velocity was reduced. The decrease of flow velocity attenuated the rate of heat transfer. When the height of partition was above 50% of the cavity height, the reduction of the heat transfer and Nusselt number were more significant.

The volume fraction of nanoparticles in the base fluid demonstrated different characteristics of fluid flow with the variation of Rayleigh number. At low Rayleigh number the use of nanoparticles augmented the rate of heat transfer while at high Rayleigh number, an adverse trend was observed.

Nomenclature

B_0	magnetic flux density
C_p	specific heat, J/kg K
g	gravitational acceleration, m/s^2
h	heat transfer coefficient, W/m^2 K
H	enclosure height, m
Ha	Hartman number
Hm	dimensionless partition height
k	thermal conductivity, W/m K
Nu	Nusselt number
p	pressure, N/m^2

P dimensionless pressure
Pr Prandtl number
q heat flux per unit area, W/m^2
Ra Rayleigh number
T temperature, K
u, v velocity components, m/s
U, V dimensionless velocity components
x, y Cartesian coordinates, m
X, Y dimensionless Cartesian coordinates

Greek symbols

α thermal diffusivity, m^2/s
β thermal expansion coefficient, K^{-1}
θ dimensionless temperature
μ dynamic viscosity, kg/m s
ν kinematic viscosity, m^2/s
ρ density, kg/m^3
σ electrical conductivity
φ volume fraction of the nanoparticles
ψ stream function

Subscripts

c cold (lower value)
f fluid
h hot (higher value)
m average
nf nanofluid
p particle

References

Ambarita, H., Kishinami, K., Maruya, M. D., Saitoh, T., Takahashi, H., & Suzuki, J. (2006). Laminar natural convection heat transfer in an air filled square cavity with two insulated baffles attached to its horizontal walls. *Thermal Science and Engineering, 14*, 35–46.

Aminossadati, S. M., & Ghasemi, B. (2009). Natural convection cooling of a localized heat source at the bottom of a nanofluid-filled enclosure. *European Journal of fluid mechanics B, 28*, 630–640.

Ampofo, F. (2004). Turbulent natural convection in an air filled partitioned square cavity. *International Journal of Heat and Fluid Flow, 25*, 103–114.

Anderson, T. N., Duke, M., & Carson, J. K. (2010). Suppression of natural convection heat transfer coefficients in an attic shaped enclosure. *International Communications in Heat and Mass Transfer, 37*, 984–986.

Arefmanesh, A., Najafi, M., & Musavi, S. H. (2013). Buoyancy-driven fluid flow and heat transfer in a square cavity with a wavy baffle – Meshless numerical analysis. *Engineering Analysis with Boundary Elements, 37*, 366–382.

Barakos, G., Mitsoulis, E., & Assimacopoulos, D. (1994). Natural convection flow in a square cavity revisited: Laminar and turbulent models with wall functions. *International Journal of Numerical Methods Fluids, 18*, 695–719.

Ben-Nakhi, A., & Chamkha, A. J. (2007). Conjugate natural convection in a square enclosure with inclined thin fin of arbitrary length. *Thermal Science and Engineering, 46*, 467–478.

Bilgen, E. (2005). Natural convection in cavities with a thin fin on the hot wall. *International Journal of Heat and Fluid Flow, 48*, 3493–3505.

Brinkman, H. C. (1952). The viscosity of concentrated suspensions and solutions. *Journal of Chemical Physics, 20*, 571–581.

De Vhal Davies, G. (1983). Natural convection of air in a square cavity: a bench mark numerical solution. *International Journal for Numerical Methods in Fluids, 3*, 227–248.

Ghasemi, B., Aminossadati, S. M., & Raisi, A. (2001). Magnetic field effect on natural convection in a nanofluid-filled square enclosure. *International Journal of Thermal Sciences, 50*, 1748–1756.

Ho, C. J., Chen, M. W., & Li, Z. W. (2008). Numerical simulation of natural convection of nanofluid in a square enclosure: Effect due to uncertainties of viscosity and thermal conductivity. *International Journal of Heat and Mass Transfer, 51*, 4506–4516.

Kahveci, K., & Oztuna, S. (2008). A differential quadrature solution of MHD natural convection in an inclined enclosure with a partition. *ASME Journal of Fluids Engineering, 130*, 021102.

Kandaswamy, P., Lee, J., Abdul Hakeem, A. K., & Saravanan, S. (2008). Effect of baffle–cavity ratios on buoyancy convection in a cavity with mutually orthogonal heated baffles. *International Journal of Heat and Mass Transfer, 51*, 1830–1837.

Khanafer, K., Vafai, K., & Lightstone, M. (2003). Buoyancy-driven heat transfer enhancement in a two-dimensional enclosure utilizing nanofluids. *International Journal of Heat and Mass Transfer, 46*, 3639–3653.

Mahmoodi, M. (2011). Numerical simulation of free convection of nanofluid in a square cavity with an inside heater. *International Journal of Thermal Sciences, 50*, 2161–2175.

Markatos, N. C., & Pericleous, K. A. (1984). Laminar and turbulent natural convection in an enclosed cavity. *International Journal of Heat and Mass Transfer, 27*, 755–772.

Maxwell-Garnett, J. C. (1904). Colours in metal glasses and in metallic films. *Philosophical Transactions of the Royal Society A: Mathematical, Physical and Engineering Sciences, 203*, 385–420.

Nada, S. A. (2007). Natural convection heat transfer in horizontal and vertical closed narrow enclosures with heated rectangular finned base plate. *International Journal of Heat and Mass Transfer, 50*, 667–679.

Oztop, H. F., & Abu-Nada, E. (2008). Numerical study of natural convection in partially heated rectangular enclosures filled with nanofluids. *International Journal of Heat and Fluid Flow, 29*, 1326–1336.

Oztop, H. F., Dagtekin, I., & Bahloul, A. (2004). Comparison of position of a heated thin plate located in a cavity for natural convection. *International Communications in Heat and Mass Transfer, 31*, 121–132.

Saravanan, S., Abdul Hakeem, A. K., & Kandaswamy, P. (2009). Natural convection in a cavity with orthogonal heat-generating baffles of different lengths. *Heat Transfer Research, 40*, 805–819.

Saravanan, S., Abdul Hakeem, A. K., Kandaswamy, P., & Lee, J. (2008). Buoyancy convection in a cavity with mutually orthogonal heated plates. *Computers and Mathematics with Applications, 55*, 2903–2912.

Wang, X., Shi, D., & Li, D. (2012). Natural convective flow in an inclined lid-driven enclosure with a heated thin plate in the middle. *International Journal of Heat and Mass Transfer, 55*, 8073–8087.